CO_2 reduction to acetic acid on the greigite Fe_3S_4{111} surface

David Santos-Carballal,[1,2,*] Alberto Roldan,[1] and Nora H. de Leeuw[1,3,2,†]

[1]*School of Chemistry, Cardiff University, Main Building, Park Place, Cardiff CF10 3AT, United Kingdom*

[2]*Present address: School of Chemistry, University of Leeds, Leeds LS2 9JT, United Kingdom*

[3]*Department of Earth Sciences, Utrecht University, Princetonplein 8A, 3584 CD Utrecht, The Netherlands*

Abstract

Acetic acid (CH_3-COOH) is an important commodity chemical widely used in a myriad of industrial processes, whose production still largely depends on homogeneous catalysts based on expensive rare metals. Here, we report a computational study on the formation of CH_3-COOH from carbon dioxide (CO_2) as an alternative chemical feedstock on the {111} surface of the low-cost greigite Fe_3S_4 catalyst. We have used density functional theory calculations with a Hubbard Hamiltonian approach and long-range dispersion corrections (DFT+U−D2) to simulate the various stages of the direct combination of C1 species of different composition to produce glyoxylic acid (CHO−COOH) as a key intermediate in the formation of CH_3-COOH. Three reaction mechanisms are considered: (*i*) the main pathway where the direct formation of the C−C bond takes place spontaneously, followed by a step-wise reduction of CHO−CHOO to CH_3-COOH; and the competitive pathways for the non-promoted and H-promoted elimination of hydroxy groups (OH) and water (H_2O), respectively from (*ii*) the carboxyl; and (*iii*) the carbonyl end of the glyoxylate intermediates. The thermodynamic and kinetic profiles show that the energies for the intermediates on the main pathway are very similar for the two catalytic sites considered, although the activation energies are somewhat larger for the exposed tetrahedral iron (Fe_A) ion. In most cases, the intermediates for the deoxygenation of the carboxylic acid are less stable than the intermediates on the main pathway, which suggests that the molecule prefers to lose the carbonylic oxygen. The suitable surface properties of the Fe_3S_4{111} surface show that this material could be a promising sustainable catalyst in future technologies for the conversion of CO_2 into organic acid molecules of commercial interest.

GRAPHICAL ABSTRACT

The greigite $Fe_3S_4\{111\}$ surface catalyses the CO_2 conversion into acetic acid (CH_3-COOH) via a glyoxylic acid ($CHO-COOH$) intermediate.

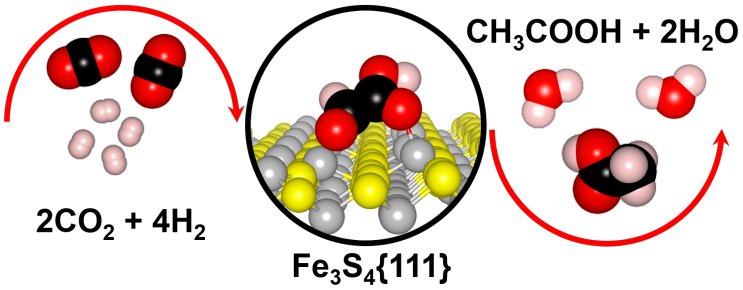

I. INTRODUCTION

Acetic acid (CH_3-COOH) is a commodity chemical with a broad spectrum of applications, including the manufacture of vinyl acetate, acetate esters, monochloroacetic acid, acetic anhydride and as a solvent in the production of dimethyl terephthalate and terephthalic acid.[1,2] Low concentration solutions of CH_3-COOH also have medical uses as an antiseptic in the local treatment of infected wounds[3–6] and in the food industry as the major solute of vinegar.[1] CH_3-COOH is important in other miscellaneous applications, such as pesticide derivatives,[7,8] the control of parasitic mites in beehives,[9] as a contrast enhancing agent in optical biopsy[10] and confocal microscopy imaging,[11] and in its hydrogenation to ethanol.[12–14] Furthermore, CH_3-COOH occurs naturally in the rain,[15–22] in the marine boundary layer air[23–25] and at diluted concentrations in several animal fluids[26] and plant systems, where it plays a key role in all biological energy pathways.[27,28]

Bacterial fermentation of ethanol (CH_3-CH_2OH) is still the preferred method for the production of the CH_3-COOH used in the pharmaceutical and food industries, given the stringent requirements of these sectors.[29] However, several synthetic routes are currently employed for the commercial production of the remaining 90% of CH_3-COOH, which is used for the majority of industrial applications. The largest scale process to produce synthetic CH_3-COOH, *i.e.* the carbonylation of methanol (CH_3OH), is a strongly exothermic reaction where carbon monoxide (CO) is catalytically inserted into the alcohol.[30] The carbonylation of methanol has been made possible largely by the use of homogeneous catalysis,

which became the leading technology in CH_3-COOH production.[31,32] Despite the excellent selectivity and activity of the iodide-promoted rhodium and iridium complex catalysts, known as Monsanto and Cativa, respectively, hydro-iodic acid (HI) is formed by the co-catalyst, which requires the use of expensive corrosion-resistant materials to construct the plant equipment.[30] The homogeneous catalysts containing costly rare metals are separated from the products through difficult catalyst recycling stream systems and continuous distillation columns. Alternative heterogeneous catalysts for the carbonylation of methanol have been described, *e.g.* supported metallic mixtures immobilised on silica and zeolites. However, the catalysts based on metallic mixtures still contain rare metals, while the use of zeolites requires a hydrolysis step and the separation of CH_3-COOH from H_2O, which is very energy-intensive and thus economically unfeasible.

Thus far, the development of stable, active and selective heterogeneous catalysts for the synthesis of CH_3-COOH remains a challenge, although it has been the subject of many investigations. The Cu{111} surface showed good catalytic performance for the insertion of CO_2 into the CH_4 molecule for the synthesis of CH_3-COOH,[33] but this was not the case for the stepped Cu{211} surface, which instead became active for the dehydrogenation of CH_3CH_2OH to CH_3-COOH.[34] Greigite (Fe_3S_4) is attracting growing interest as an environmentally acceptable and inexpensive catalyst since it has been shown to convert CO_2 into small amounts of various C1 species, CH_3-COOH and pyruvic acid ($CH_3COCOOH$).[35] Fe_3S_4 is ubiquitous in ancient soil[36,37] and marine environments,[38,39] where it has been linked to the "iron-sulfur world" origin of life theory.[40,41] This concept suggests that Fe_3S_4, amongst other metal sulfides, was instrumental in catalysing the reduction of CO_2 into the first organic molecules following a number of biochemical reactions involving the oxidation of the Fe^{2+} ions. However, the mechanistic pathway for the formation of the C−C bond, or the selective reduction of intermediates, are not yet fully understood. Insight into these processes is critical if we are to exploit Fe_3S_4 as a catalyst, not only for the synthesis of CH_3-COOH, but also to utilise the greenhouse gas CO_2 as a readily available chemical feedstock.

Given the importance of CH_3-COOH as a precursor of industrial polymeric materials of commercial significance and the disadvantages of its current synthesis methods, in this paper we describe a novel approach for the production of this chemical. Inspired by the reported catalytic activity of the Fe_3S_4{111} surface towards the activation of the CO_2 molecule and the interest in reducing its concentration in the atmosphere, we have used density functional

theory (DFT) calculations to study the formation of CH_3-COOH on the active facet of this spinel-structured iron sulfide. We analyse the interaction and direct combination of several C1 species on the $Fe_3S_4\{111\}$ surface and we propose three mechanistic pathways to account for the formation of one C−C bond between two C1 species and deoxygenation of the intermediates. This approach has allowed us to explore the complete thermodynamic and kinetic profiles for the formation of CH_3-COOH over the $Fe_3S_4\{111\}$ surface using CO_2 as the chemical feedstock.

II. COMPUTATIONAL METHODS

A. Calculation details

Periodic plane-wave DFT calculations were carried out to study the production of acetic acid from the hydrogenation of CO_2 on the greigite surface. All calculations were performed using the Vienna Ab Initio Simulation Package (VASP).[42–45] Ion–electron interactions were represented by the projector-augmented wave (PAW) method[46,47] and the generalized gradient approximation (GGA) with the Perdew–Wang 91 (PW91) functional[48,49] within the spin interpolation formula of Vosko *et al.*[50] We have also considered non-spherical contributions from the gradient corrections to the PAW spheres. All calculations include the D2 long-range dispersion correction approach by Grimme,[51] which is an improvement on standard DFT when considering large polarisable atoms.[52–59] We have used the global scaling factor parameter optimized for the Perdew, Burke and Ernzerhof (PBE)[60,61] functional, ($s_6 = 0.75$). Different long-range dispersion correction approximations and DFT functionals have been tested in the iso-structural spinel violarite $FeNi_2S_4$, but these led to only minor differences of the surface energy and adsorption energy for the CO_2 molecule.[57] The Kohn-Sham valence states were expanded in a plane-waves basis set with a cut off of 600 eV for the kinetic energy. This high value for the cut-off energy ensured that no Pulay stresses occurred within the cell during relaxations.

The initial magnetic moment was described by high-spin distributions in both octahedral and tetrahedral types of Fe, with the antiparallel orientation previously used for the spinel structure,[52–58] which results in a ferromagnetic material.[62–69] The orbital spin-splitting in the valence region results in localized outermost $3d$-electrons and in ordered magnetism.[63,70,71]

Good agreement with experimental evidence has been obtained by using the same computational details as listed above.[52–58] For an accurate treatment of the electron correlation in the localized *d*-Fe orbital, we have used the U approximation[72,73] ($U_{\text{eff}} = 1$ eV),[52,55–58,69,74,75] which improves the description of localized states in this type of systems where standard local density approximation (LDA) and GGA functionals fail.[76] The choice of the U parameter is rather empirical, which is also a common feature of the computationally expensive hybrid functionals, since the amount of Fock exchange is system-dependent.[76–79] Calculations were carried out using a Γ-centered Monkhorst-Pack grid of $5 \times 5 \times 1$ k-points, which ensures the electronic and ionic convergence.[80] The geometry of all stationary points was found with the conjugate-gradient algorithm and considered converged when the force on each ion dropped below 0.03 eV Å^{-1}. The energy threshold defining self-consistency of the electron density was set to 10^{-5} eV. In order to improve the convergence of the Brillouin-zone integrations, the partial occupancies were determined using the tetrahedron method with Blöch corrections.[81]

B. Surface models

The Fe_3S_4 unit cell consists of eight formula units with a cubic lattice parameter of ∼9.8 Å,[82,83] which is close to the value resulting from the cell optimization (9.671 Å). The inverse thio-spinel arrangement is reflected by the formula AB_2S_4, where there are two possible locations for the Fe ions: the tetrahedral sites (A), filled by Fe^{3+} ions, and the octahedral sites (B), with equal quantities of both Fe^{3+} and Fe^{2+} ions.[63,64,66–68,70,74] We have prepared the $Fe_3S_4\{111\}$ surface as a slab model by cutting the bulk structure with the METADISE code,[84] which considers periodicity in the plane direction and provides the atomic layer stacking resulting in non-dipolar reconstructions.[85] The {111} surface slab contains 56 atoms (24 Fe and 32 S) distributed in 9 layers, of which the 5 bottom-most were kept fixed at their bulk positions, and exposes an area of 81.0 Å^2 per unit cell. Different slab thicknesses and numbers of relaxed layers were tested until convergence within 1 meV per cell was achieved. We added a vacuum width of 12 Å between the periodic slabs, which is big enough to avoid interaction between them.

C. Thermodynamic and kinetic profiles

The initial and final states of the reduction process by hydrogenation and elimination of H_2O or OH and the C−C bond formation are linked by a saddle point in the pathway of minimum energy across the potential surface. The reaction transition states (TS's) are found at these saddle points, leading to the energy barriers that reactants need to overcome before forming the products. The TS's, which determine the kinetics of the process, were identified by means of the dimer method,[86,87] and characterised by vibrational frequency calculations, in which only one imaginary mode is obtained, corresponding to the reaction coordinate.

The activation energy (E_A) of a certain step is the energy required to surmount the potential barrier characteristic of the transition state. This energy barrier is defined as the difference between the initial and transition state energies for the forward process. The reaction energy (E_R) of each step is calculated as the total energy difference between the final state, *i.e.* product(s), and the initial state, *i.e.* reactant(s). The E_R provides information regarding the thermodynamic feasibility of the process.

III. RESULTS AND DISCUSSION

Fe_3S_4, the sulfide counterpart of the spinel-structured iron oxide magnetite (Fe_3O_4), displays different crystal morphologies depending on the synthesis conditions. Notably, the hydrothermal synthesis method leads almost exclusively to the {001} and {111} surfaces in the Fe_3S_4 nano-particles.[88] Recently, we have shown the conversion of CO_2 into small organic molecules as catalysed by the active termination of the $Fe_3S_4\{111\}$,[35] where the different Fe_A and Fe_B sites were selective towards the formation of specific products. The {111} surface termination has a bulk-like structure consisting of double rows of S ions along the $[0\bar{1}1]$ direction and with rhombohedral packing alternating with a single row of Fe_A cations. The polarity of this surface termination is quenched by a 0.5 monolayer (ML) of three-fold Fe_B atoms sited in the hexagonal close-packed *hcp* hollow positions with $p(1 \times 2)$ symmetry.

We have considered the formation of CH_3-COOH using CO_2 and H_2 as the source of all the atomic elements required for this process. CO_2 is adsorbed linearly on the $Fe_3S_4\{111\}$ surface with a binding energy of -0.62 eV,[35] while the H_2 molecule dissociates upon adsorp-

TABLE I. Relative energies (ΔE), for the C1 species CHO, COH, CHOO and COOH on the Fe_A and Fe_B sites of the $Fe_3S_4\{111\}$ surface.

Species	ΔE (eV)	
	Fe_A	Fe_B
CHO	0.00	0.00
COH	1.52	1.74
CHOO	0.25	0.33
COOH	0.00	0.00

tion, releasing −0.63 eV. Given the presence of CO_2 and H ad-atoms at the Fe_3S_4 catalyst, the equilibrium for the reverse water-gas shift reaction allows the evolution of CO and H_2O. The H ad-atoms can subsequently react with both co-adsorbed CO and CO_2 to form CHO and COOH, respectively, which are the precursors to CH_3–COOH in our proposed pathways. Table I displays the relative energies of the four mono-protonated C1 species, showing that adsorbed CHO and COOH are the most stable, which supports our choice of precursors.

A. Direct combination of the CHO and COOH surface species

Fig. 1 displays the process of direct combination between the CHO and COOH species on the $Fe_3S_4\{111\}$ surface. The C atom of both reactants sits atop the surface cations at a distance of ∼2.0 Å, shorter on the Fe_B than on the Fe_A site, which is in agreement with previous works.[89] Despite the existence of several possibilities for the co-adsorption of CHO and COOH on the $Fe_3S_4\{111\}$ surface, we have left them sited on the neighbouring Fe_A and Fe_B atoms, which are the thermodynamically most favourable positions, see Table I. In a direct concerted step, the two fragments combine to form glyoxylic acid (CHO−COOH) and the carbonyl end of the molecule detaches from the surface. This is an exothermic process with a reaction energy of −3.08 eV and an activation energy of 2.26 eV. During formation of the C−C bond, CHO−COOH regains 80% of the charge previously transferred to the surface, in agreement with the thermodynamic stability of this molecule. This reaction is not isogyric and it is, thus, spin-forbidden in the gas phase, as the total electron spin is not conserved, *i.e.* the radical reactants exist in spin state $s = 1$ and the diamagnetic product exist in $s = 0$. This difficulty further supports the use of catalysts containing transition

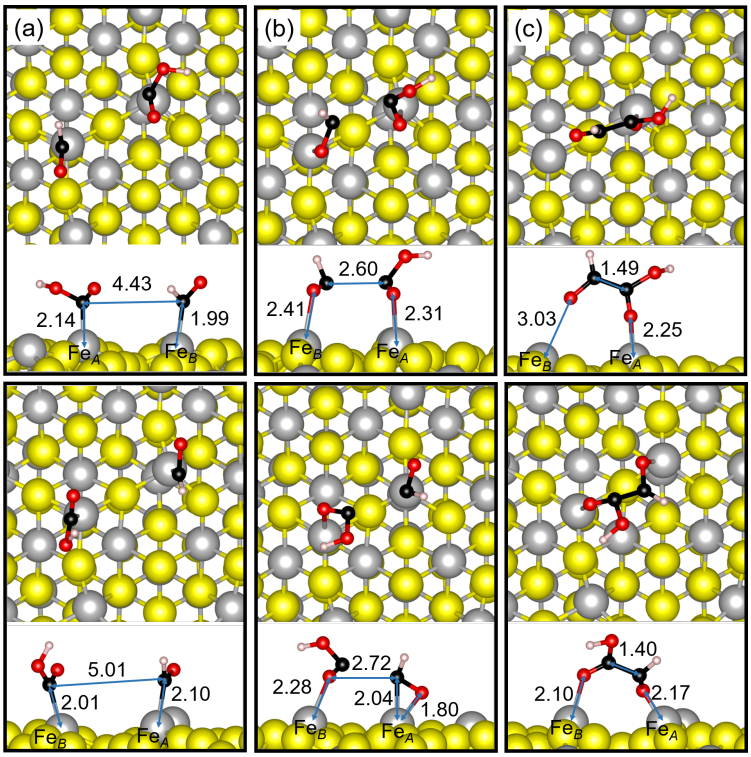

FIG. 1. Top and side views of the (a) initial, (b) transition and (c) final states for the direct combination of CHO and COOH on the Fe_A (top panels) and Fe_B site (bottom panels) of the $Fe_3S_4\{111\}$ surface. Fe is in light-grey, S is in yellow, O is in red, H is in white and C is in black. Calculated bond distances are shown in Å.

metals for the synthesis of CH_3-COOH, as they can induce spin changes that can overcome the spin-prohibition.[90,91]

Despite extensive computational and experimental studies of the interaction between CH_3-COOH and different types of surfaces, the adsorption of $CHO-COOH$ has so far been overlooked in the literature. The adsorption energy for CH_3-COOH has been reported to lie between -0.84 and -0.30 eV on the $\{111\}$ surface of pure Cu and its alloys with other transition metals.[92] However, on oxides such as CeO_2, the adsorption energies are -0.95 and -2.50 eV for the stoichiometric material and for a material with oxygen vacancies, respectively,[93] indicating that the organic acid prefers the interaction with positive surface sites. We speculate that less ionic materials, such as Fe_3S_4, can interact with C2 organic acids and release adsorption energies between the typical values of metals and metal oxides. This ensures that the reactant adsorbates are anchored to the catalytic sites with enough

strength for the reaction to take place, while still allowing the products to leave the surface, thereby freeing up the catalytic site.

B. Adsorption of glyoxylate intermediate species

We have simulated the adsorption of a number of glyoxylic acid intermediates in the formation of CH_3-COOH, containing an increasing number of H atoms, as shown in Table II. Apart from $CHO-COOH$ and CH_3-COOH, all surface intermediates have higher energies, although they are never larger than 1.59 eV with respect to the reactants and products. Our calculations also suggest that the C−C bond length undergoes minor changes along the reduction process, which are particularly noticeable in the $H_2C(OH)-COOH$ species. The Fe−C distance, as well as the stretching vibrational mode υ_{C-C} are only negligibly affected during the protonation reactions. In this work, the hybridisation of the carbonyl carbon atom changes only from sp^2 to sp^3, which causes the structural properties to change less than the largest change from sp^1 to sp^3 seen in our previous report on the conversion of CO into methanol CH_3OH.[89] The adsorption configuration of $CHO-COOH$ and its protonated species are characterised by the non-protonated carboxyl oxygen coordinating the metal sites of the surface at 2.10 to 2.85 Å, which is on average 0.2 Å longer than the Fe−C distance calculated for the C1 species.

C. Elimination of H_2O and OH from the glyoxylate intermediate species

We have studied the deoxygenation of the species on the Fe_A and Fe_B sites, where the products remain at the same adsorption position, *e.g.* the dissociation of the C-OH bond from the carboxylic part of $CHO-COOH$ on Fe_A leads to $CHO-CO$ at the same site, as the coordination to the surface takes place through the non-protonated carboxyl oxygen, see Fig. 2. Following the elimination of the OH group, the $CHO-CO$ species moves an average of 0.1 Å closer to surface metal site than before dissociation. The trend in the distance between the deoxygenated species and the surface can be rationalised in terms of the amount of positive charge of the latter. This is induced by the electrophilic co-adsorbed OH groups that have just left the intermediate, which gain electrons from the neighbouring atoms of the catalytic site.

TABLE II. Relative energies (ΔE), distances (d) and stretching vibrational modes (υ) for the C−C bond of the different glyoxylate intermediate species adsorbed on the Fe_A and Fe_B sites of the Fe_3S_4{111} surface. The energies of the intermediates are relative to adsorbed glyoxylic acid, considering the contribution from the corresponding number of H ad-atoms.

Label	Adsorbate	ΔE (eV)		d_{C-C} (Å)		d_{Fe-O} (Å)		υ_{C-C} (cm^{-1})	
		Fe_A	Fe_B	Fe_A	Fe_B	Fe_A	Fe_B	Fe_A	Fe_B
$a1$	CHO−COOH	0.00	0.00	1.491	1.403	2.104	2.252	849	853
$a2$	CH(OH)−COOH	−0.68	−0.72	1.354	1.431	2.363	2.429	872	848
$a3$	CH_2O−COOH	−1.40	−1.25	1.518	1.314	2.287	2.371	837	887
$a4$	CH_2(OH)−COOH	−2.26	−1.87	1.464	1.441	2.194	2.488	860	829
$a5$	CH_2−COOH	−2.51	−2.15	1.418	1.386	2.371	2.283	826	784
$a6$	CH_3−COOH	−3.36	−3.48	1.392	1.487	2.850	2.580	862	874

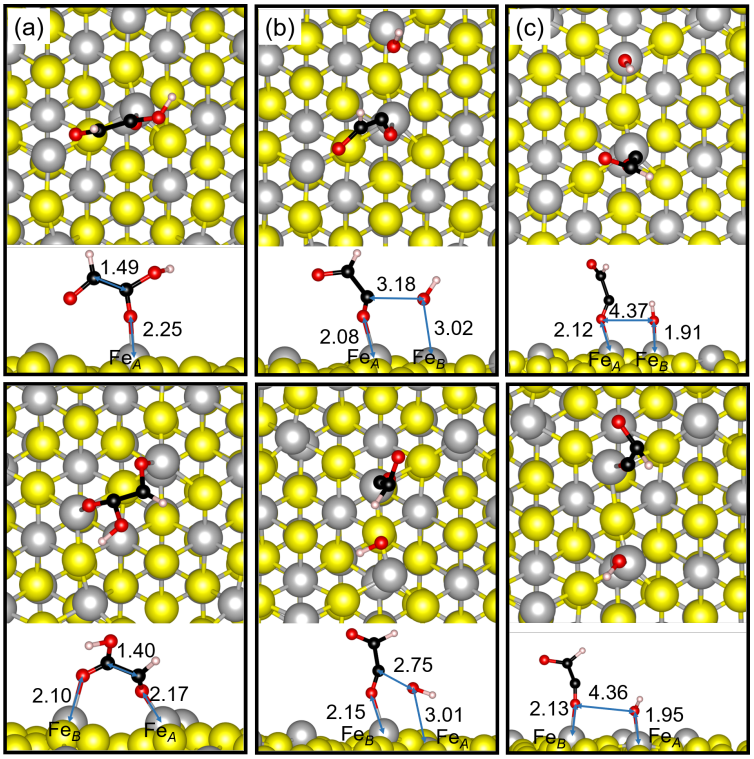

FIG. 2. Top and side views of the (a) initial, (b) transition and (c) final states for the elimination of OH from CHO−COOH on the Fe_A (top panels) and Fe_B (bottom panels) sites of the Fe_3S_4{111} surface. Fe is in light-grey, S is in yellow, O is in red, H is in white and C is in black. Calculated bond distances are shown in Å.

TABLE III. Activation ($E_{\rm A}$) and reaction ($E_{\rm R}$) energies for the elimination of OH from the glyoxylate intermediate species on the Fe_A and Fe_B sites of the $Fe_3S_4\{111\}$ surface

Label	Reactants		Products	$E_{\rm A}$ (eV)		$E_{\rm R}$ (eV)	
				Fe_A	Fe_B	Fe_A	Fe_B
$R1$	CHO−COOH	→	CHO−CO + OH	3.83	4.12	2.14	3.06
$R2$	CH(OH)−COOH	→	CH(OH)−CO + OH	2.58	1.67	1.33	1.38
$R3$	CH_2O−COOH	→	CH_2O−CO + OH	1.42	2.81	0.20	0.12
$R4$	CH_2(OH)−COOH	→	CH_2(OH)−CO + OH	1.73	2.35	−0.34	0.87
$R5$	CH_2−COOH	→	CH_2−CO + OH	2.31	2.04	0.15	1.53
$R6$	CH_3−COOH	→	CH_3−CO + OH	1.26	2.63	0.26	0.72

Table III displays the activation and reaction energies for the non-promoted dissociation of the C−OH bond from the carboxylic end of the intermediates. On the Fe_A catalytic sites, the reaction energy ($E_{\rm R}$) associated with the scission of the C−OH bond are (*i*) endothermic ($0.15\ {\rm eV} < E_{\rm R} < 2.14\ {\rm eV}$) for the $R1$, $R2$, $R3$, $R5$ and $R6$ species, and (*ii*) exothermic ($E_{\rm R} < 0$ eV) for $R4$. However, the large potential energy of the transition states suggest that these reactions are kinetically unfeasible and that the dissociation of the C−OH bond is unlikely. Moreover, the smallest $E_{\rm A}$ was calculated for the formation of CH_3−COOH, although it is still larger than 1.25 eV. The different coordination environment of the Fe_B catalytic site dictates a different behaviour, as all non-promoted dissociations of the C−OH bond are endothermic with activation energies larger than 1.5 eV.

We have also simulated the elimination of the carboxylic OH group promoted by H, which is displayed in Fig. 3. Table IV shows the calculated $E_{\rm A}$ and $E_{\rm R}$ for these reactions, where one H_2O molecule is formed and released. In general, our calculations indicate that $E_{\rm R}$ are endothermic but that they decrease with the degree of protonation of the intermediate for both the Fe_A and Fe_B catalytic sites. However, the formation of the cyclic acetolactone CH_2O−CO intermediate is slightly exothermic, as one of the O atoms bonds simultaneously to the two C atoms leading to full-coordination of all atoms. Similarly, the reaction energy for CH_2(OH)−CO is $E_{\rm R} < 0$ given that the hydroxylated C is fully saturated and the molecule rotates to bind to the surface through the carbonyl C. However, notwithstanding the favourable structural changes of some reduced intermediates, their formation processes

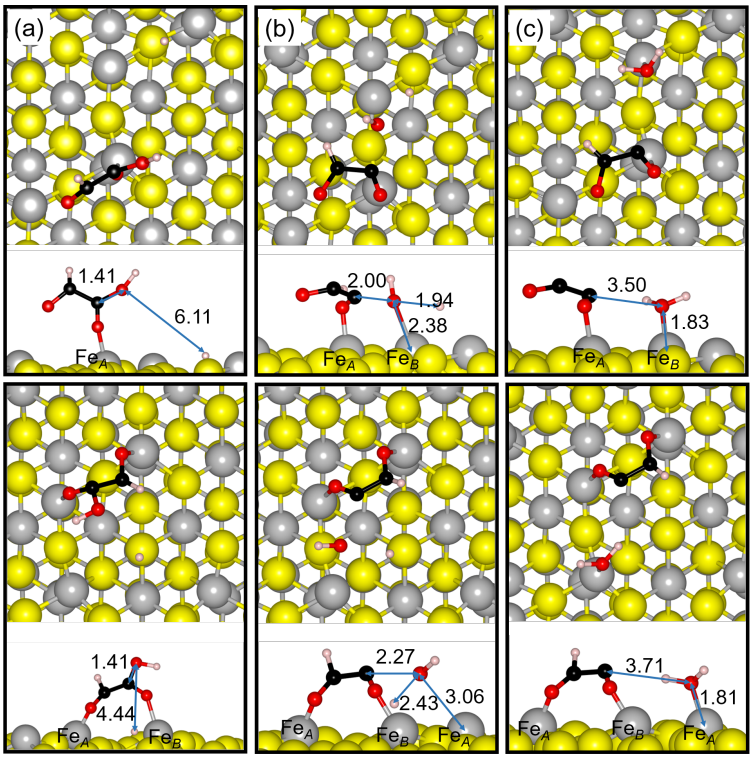

FIG. 3. Top and side views of the (a) initial, (b) transition and (c) final states for the H-promoted elimination of H_2O from CHO−COOH on the Fe_A (top panels) and Fe_B (bottom panels) sites of the Fe_3S_4{111} surface. Fe is in light-grey, S is in yellow, O is in red, H is in white and C is inblack. Calculated bond distances are shown in Å.

still have large activation energies, which makes them kinetically unlikely to happen.

D. Mechanism and reaction profiles

Fig. 4 illustrates the energy profiles for the main reaction, *i.e.* the reduction of CHO−COOH to CH_3−COOH, alongside the competitive pathways studied for the non-promoted and the H-promoted dissociation of the C−OH bond in the carboxylic end of the molecule. As already discussed, the majority of the elementary steps within these paths are hindered by the large potential energies of the transition states, which makes the alternative pathways particularly difficult to attain. However, the products of the competitive process R4 is more stable than the products of the main reaction, suggesting that the elimination of H_2O and OH from the carboxyl end of the molecule are possible if the system receives enough energy to overcome the transition states.

TABLE IV. Activation (E_{A}) and reaction (E_{R}) energies for the elimination of H_2O from the glyoxylate intermediate species on the Fe_A and Fe_B sites of the $Fe_3S_4\{111\}$ surface

Reaction	Reactants		Products	E_{A} (eV)		E_{R} (eV)	
				Fe_A	Fe_B	Fe_A	Fe_B
$R7$	CHO−COOH + H	→	CHO−CO + H_2O	1.64	2.58	0.73	1.12
$R8$	CH(OH)−COOH + H	→	CH(OH)−CO + H_2O	0.98	1.72	0.78	0.69
$R9$	CH_2O−COOH + H	→	CH_2O−CO + H_2O	1.53	1.96	−0.23	−0.24
$R10$	CH_2(OH)−COOH + H	→	CH_2(OH)−CO + H_2O	1.85	1.72	−0.17	−0.21
$R11$	CH_2−COOH + H	→	CH_2−CO + H_2O	1.72	1.67	0.61	0.44
$R12$	CH_3−COOH + H	→	CH_3−CO + H_2O	1.96	1.82	0.64	0.57

Although the main pathway involves several glyoxylate intermediate species, the reactions take different courses on the two catalytic sites that we have considered. For example, on the Fe_A site, the main reaction will proceed via the intermediates $a1$, $a3$, $a4$, $a5$ and $a6$ because of their stability and the low activation energies of the transition states that connect them. Despite the 0.72 eV energy difference between $a2$ and $a3$, the elementary steps for converting $a3$ into $a5$ requires less energy than the transformation of $a2$ or $a3$ into $a4$. On the other hand, the transition states have the largest barrier for the elimination of H_2O and OH from the intermediates adsorbed on the Fe_B site, implying that these processes are less likely to occur than on the Fe_A site. Notably, the reaction network for the Fe_B site shows less inter-crossing of the transition and final states than that for the Fe_A site.

IV. CONCLUSIONS

In this study, we have carried out a comprehensive simulation of the conversion of CO_2 into CH_3−COOH on both adsorption sites Fe_A and Fe_B of the $Fe_3S_4\{111\}$ surface. We have modelled the formation of CO as a result of the reverse water-gas shift reaction. The two oxygenated C1 species were subsequently protonated by a H ad-atom leading to CHO and COOH, which are the precursors of CHO−COOH, a key intermediate in the formation of CH_3−COOH. The mechanistic profiles show that the transformation of CHO−COOH into CH_3−COOH is thermodynamically feasible, owing to the large energy of the H_2 molecule

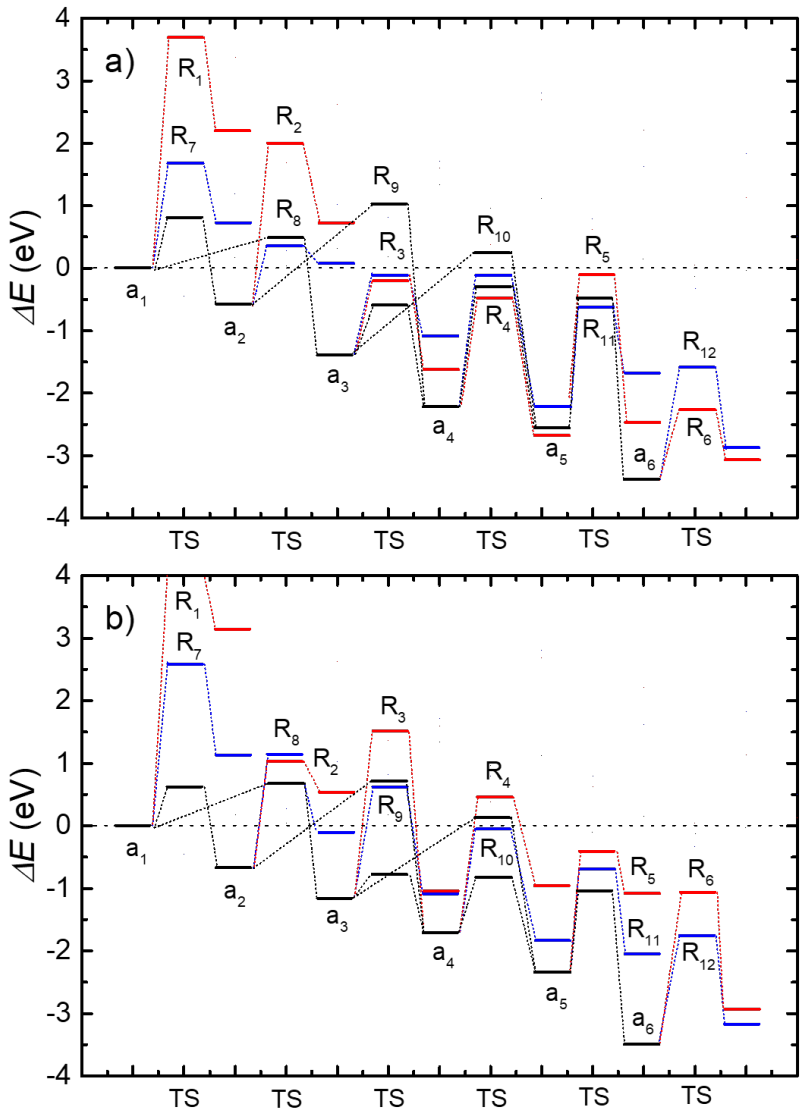

FIG. 4. Energy profile for (black line) the reduction mechanism of CHO−CHOO to CH_3−COOH on the (a) Fe_A and (b) Fe_B sites of the Fe_3S_4{111} surface; alongside the competitive (red line) non-promoted and (blue line) H-promoted elimination of OH and H_2O, respectively. Intermediates and reaction labels are provided according to Tables 1-3.

and the elimination of H_2O. The reaction barriers for the protonation are smallest for the intermediates where the carbonyl oxygen is protonated, as the carbon atom directly attached is able to easily accept H atoms and to lose one H_2O molecule. We have also investigated the protonation and elimination of one of the oxygen atoms from the carboxylic group during the reduction process of CHO−COOH. In general, the formation of glyoxal or ethylene glycol are unfavourable processes as these products are less stable than the intermediates from the

main reduction process, indicating that the $Fe_3S_4\{111\}$ surface is highly selective towards the reduction of the carbonyl rather than the carboxyl end of the molecule, which ultimately leads to CH_3-COOH.

AUTHOR INFORMATION

ORCID:

David Santos-Carballal: 0000-0002-3199-9588
Alberto Roldan: 0000-0003-0353-9004
Nora H. de Leeuw: 0000-0002-8271-0545

CONFLICTS OF INTEREST

There are no conflicts to declare.

ACKNOWLEDGEMENTS

We acknowledge the Engineering and Physical Sciences Research Council (EPSRC grants EP/K009567/2, EP/K035355/2 and EP/K001329/1) for funding. Through our membership of the UK's HEC Materials Chemistry Consortium, which is funded by EPSRC (EP/L000202), this work used the ARCHER UK National Supercomputing Service (`http://www.archer.ac.uk`). This work was performed using the computational facilities of the Advanced Research Computing @ Cardiff (ARCCA) Division, Cardiff University. The authors also acknowledge the use of HPC Wales, Supercomputing Wales, and associated support services in the completion of this work. All data created during this research is openly available from the Cardiff University's Research Portal at `https://doi.org/10.17035/d.2020.0040949136`.

---

* E-mail: SantosCarballalD@cardiff.ac.uk, D.Santos-Carballal@leeds.ac.uk; Tel: +44 (0)29 2087 4715

† E-mail: deLeeuwN@cardiff.ac.uk, N.H.deLeeuw@leeds.ac.uk; Tel: +44 (0)29 2087 0658, +44 (0)11 3343 9008

[1] F. S. Wagner and Updated by Staff, in *Kirk-Othmer Encycl Chem Technol*, John Wiley & Sons, Inc., Hoboken, NJ, USA, 2014, pp. 1–21.

[2] C. Le Berre, P. Serp, P. Kalck and G. P. Torrence, in *Ullmann's Encycl Ind Chem*, Wiley-VCH Verlag GmbH & Co. KGaA, Weinheim, Germany, 2014, vol. 74, pp. 1–34.

[3] I. Phillips, A. Lobo, R. Fernandes and N. Gundara, *Lancet*, 1968, **291**, 11–13.

[4] J. M. Sloss, N. Cumberland and S. M. Milner, *J R Army Med Corps*, 1993, **139**, 49–51.

[5] H. Ryssel, O. Kloeters, G. Germann, T. Schäfer, G. Wiedemann and M. Oehlbauer, *Burns*, 2009, **35**, 695–700.

[6] K. Taylor, *J Am Med Assoc*, 1916, **LXVII**, 1598.

[7] A. V. Ogram, R. E. Jessup, L. T. Ou and P. S. Rao, *Appl Environ Microbiol*, 1985, **49**, 582–587.

[8] M. Qamar and M. Muneer, *J Hazard Mater*, 2005, **120**, 219–227.

[9] D. Van Engelsdorp, R. M. Underwood and D. L. Cox-foster, *J Econ Entomol*, 2008, **101**, 256–264.

[10] C. J. Balas, G. C. Themelis, E. P. Prokopakis, I. Orfanudaki, E. Koumantakis and E. S. Helidonis, *J Photochem Photobiol B Biol*, 1999, **53**, 153–157.

[11] R. A. Drezek, T. Collier, C. K. Brookner, A. Malpica, R. Lotan, R. R. Richards-Kortum and M. Follen, *Am J Obstet Gynecol*, 2000, **182**, 1135–1139.

[12] W. Rachmady and M. A. Vannice, *J Catal*, 2000, **192**, 322–334.

[13] W. Rachmady and M. A. Vannice, *J Catal*, 2002, **207**, 317–330.

[14] V. Pallassana and M. Neurock, *J Catal*, 2002, **209**, 289–305.

[15] J. N. Galloway, G. E. Likens, W. C. Keene and J. M. Miller, *J Geophys Res*, 1982, **87**, 8771.

[16] W. C. Keene, J. N. Galloway and J. D. Holden, *J Geophys Res Ocean*, 1983, **88**, 5122–5130.

[17] S. F. Guiang, S. V. Krupa and G. C. Pratt, *Atmos Environ*, 1984, **18**, 1677–1682.

[18] W. C. Keene and J. N. Galloway, *Atmos Environ*, 1984, **18**, 2491–2497.

[19] R. B. Norton, *Geophys Res Lett*, 1985, **12**, 769–772.

[20] W. C. Keene and J. N. Galloway, *J Geophys Res*, 1986, **91**, 14466.

[21] M. O. Andreae, R. W. Talbot, T. W. Andreae and R. C. Harriss, *J Geophys Res*, 1988, **93**, 1616.

[22] J. D. Willey and C. A. Wilson, *J Atmos Chem*, 1993, **16**, 123–133.

[23] E. D. Baboukas, M. Kanakidou and N. Mihalopoulos, *J Geophys Res Atmos*, 2000, **105**, 14459–14471.

[24] R. B. Norton, *J Geophys Res*, 1992, **97**, 10389.

[25] M. Legrand, S. Preunkert, B. Jourdain and B. Aumont, *J Geophys Res Atmos*, 2004, **109**, n/a–n/a.

[26] K. Bloch and D. Rittenberg, *J Biol Chem*, 1944, **155**, 243–254.

[27] C. Bianco, *Microbiology*, 2006, **152**, 2421–2431.

[28] A. Östin, M. Kowalyczk, R. P. Bhalerao and G. Sandberg, *Plant Physiol*, 1998, **118**, 285–296.

[29] R. J. Gomes, M. d. F. Borges, M. d. F. Rosa, R. J. H. Castro-Gómez and W. A. Spinosa, *Food Technol Biotechnol*, 2018, **56**, 139–151.

[30] A. Haynes, in *Adv Catal*, 2010, pp. 1–45.

[31] D. Forster, in *Adv Organomet Chem*, 1979, pp. 255–267.

[32] T. W. Dekleva and D. Forster, in *Adv Catal*, 1986, pp. 81–130.

[33] R. Zhang, L. Song, H. Liu and B. Wang, *Appl Catal A Gen*, 2012, **443-444**, 50–58.

[34] B. Voss, N. C. Schjødt, J. D. Grunwaldt, S. I. Andersen and J. M. Woodley, *Appl Catal A Gen*, 2011, **402**, 69–79.

[35] A. Roldan, N. Hollingsworth, A. Roffey, H.-U. Islam, J. B. M. Goodall, C. R. A. Catlow, J. A. Darr, W. Bras, G. Sankar, K. B. Holt, G. Hogarth and N. H. de Leeuw, *Chem Commun*, 2015, **51**, 7501–7504.

[36] J. W. E. Fassbinder and H. Stanjek, *Geophys Res Lett*, 1994, **21**, 2349–2352.

[37] J. W. E. Fassbinder, H. Stanjek and H. Vali, *Nature*, 1990, **343**, 161–3.

[38] A. P. Roberts and G. M. Turner, *Earth Planet Sci Lett*, 1993, **115**, 257–273.

[39] A. Jelinowska, P. Tucholka, F. Guichard, I. Lefevre, F. Gasse, N. Tribovillard, A. Desprairies and F. Chalie, *Geophys J Int*, 1998, **133**, 499–509.

[40] M. J. Russell and A. J. Hall, *J Geol Soc London*, 1997, **154**, 377–402.

[41] G. Wächtershäuser, *Prog Biophys Mol Biol*, 1992, **58**, 85–201.

[42] G. Kresse and J. Hafner, *Phys Rev B*, 1993, **47**, 558–561.

[43] G. Kresse and J. Hafner, *Phys Rev B*, 1994, **49**, 14251–14269.

[44] G. Kresse and J. Furthmüller, *Phys Rev B*, 1996, **54**, 11169–11186.

[45] G. Kresse and J. Furthmüller, *Comput Mater Sci*, 1996, **6**, 15–50.

[46] P. E. Blöchl, *Phys Rev B*, 1994, **50**, 17953–17979.

[47] G. Kresse and D. Joubert, *Phys Rev B*, 1999, **59**, 1758–1775.

[48] J. P. Perdew, J. A. Chevary, S. H. Vosko, K. A. Jackson, M. R. Pederson, D. J. Singh and C. Fiolhais, *Phys Rev B*, 1992, **46**, 6671–6687.

[49] J. P. Perdew, J. A. Chevary, S. H. Vosko, K. A. Jackson, M. R. Pederson, D. J. Singh and C. Fiolhais, *Phys Rev B*, 1993, **48**, 4978–4978.

[50] S. H. Vosko, L. Wilk and M. Nusair, *Can J Phys*, 1980, **58**, 1200–1211.

[51] S. Grimme, *J Comput Chem*, 2006, **27**, 1787 – 1799.

[52] A. Roldan, D. Santos-Carballal and N. H. de Leeuw, *J Chem Phys*, 2013, **138**, 204712.

[53] D. Santos-Carballal, A. Roldan, R. Grau-Crespo and N. H. de Leeuw, *Phys Chem Chem Phys*, 2014, **16**, 21082–21097.

[54] D. Santos-Carballal, A. Roldan, R. Grau-Crespo and N. H. de Leeuw, *Phys Rev B*, 2015, **91**, 195106.

[55] D. Santos-Carballal, A. Roldan and N. H. de Leeuw, *J Phys Chem C*, 2016, **120**, 8616–8629.

[56] D. Santos-Carballal, A. Roldan, N. Y. Dzade and N. H. de Leeuw, *Philos Trans R Soc A Math Phys Eng Sci*, 2018, **376**, 20170065.

[57] S. Posada-Pérez, D. Santos-Carballal, U. Terranova, A. Roldan, F. Illas and N. H. de Leeuw, *Phys Chem Chem Phys*, 2018, **20**, 20439–20446.

[58] S. N. A. Zakaria, N. Hollingsworth, H. Islam, A. Roffey, D. Santos-Carballal, A. Roldan, W. Bras, G. Sankar, G. Hogarth, K. B. Holt and N. H. de Leeuw, *ACS Appl Mater Interfaces*, 2018, **10**, 32078–32085.

[59] M. J. Ungerer, D. Santos-Carballal, A. Cadi-Essadek, C. G. C. E. van Sittert and N. H. de Leeuw, *J Phys Chem C*, 2019, acs.jpcc.9b06136.

[60] J. P. Perdew, K. Burke and M. Ernzerhof, *Phys Rev Lett*, 1996, **77**, 3865–3868.

[61] J. P. Perdew, K. Burke and M. Ernzerhof, *Phys Rev Lett*, 1997, **78**, 1396–1396.

[62] D. Vaughan and M. Ridout, *J Inorg Nucl Chem*, 1971, **33**, 741–746.

[63] D. J. Vaughan and J. A. Tossell, *Am Mineral*, 1981, **66**, 1250–1253.

[64] D. J. Vaughan and J. A. Tossell, *Phys Chem Miner*, 1983, **9**, 253–262.

[65] M. Braga, S. K. Lie, C. A. Taft and W. A. J. Lester, *Phys Rev B*, 1988, **38**, 10837–10851.

[66] K. K. Surerus, M. C. Kennedy, H. Beinert and E. Münck, *Proc Natl Acad Sci U S A*, 1989, **86**, 9846–9850.

[67] M. J. Dekkers and M. A. A. Schoonen, *Geophys J Int*, 1996, **126**, 360–368.

[68] M. J. Dekkers, H. F. Passier and M. A. A. Schoonen, *Geophys J Int*, 2000, **141**, 809–819.

[69] L. Chang, A. P. Roberts, Y. Tang, B. D. Rainford, A. R. Muxworthy and Q. Chen, *J Geophys Res*, 2008, **113**, B06104.

[70] D. J. Vaughan and J. R. Craig, *Am Mineral*, 1985, **70**, 1036–1043.

[71] D. Rickard and G. W. Luther III, *Chem Rev (Washington, DC, United States)*, 2007, **107**, 514–62.

[72] V. I. Anisimov, M. A. Korotin, J. Zaanen and O. K. Andersen, *Phys Rev Lett*, 1992, **68**, 345–348.

[73] S. L. Dudarev, G. A. Botton, S. Y. Savrasov, C. J. Humphreys and A. P. Sutton, *Phys Rev B*, 1998, **57**, 1505–1509.

[74] L. Chang, B. D. Rainford, J. R. Stewart, C. Ritter, A. P. Roberts, Y. Tang and Q. Chen, *J Geophys Res*, 2009, **114**, B07101.

[75] A. J. Devey, R. Grau-Crespo and N. H. de Leeuw, *Phys Rev B*, 2009, **79**, 195126.

[76] I. d. P. R. Moreira, F. Illas and R. L. Martin, *Phys Rev B*, 2002, **65**, 155102.

[77] I. Ciofini, F. Illas and C. Adamo, *J Chem Phys*, 2004, **120**, 3811–3816.

[78] F. Illas and R. L. Martin, *J Chem Phys*, 1998, **108**, 2519–2527.

[79] D. Muñoz, N. Harrison and F. Illas, *Phys Rev B*, 2004, **69**, 085115.

[80] H. J. Monkhorst and J. D. Pack, *Phys Rev B*, 1976, **13**, 5188–5192.

[81] P. E. Blöchl, O. Jepsen and O. K. Andersen, *Phys Rev B*, 1994, **49**, 16223–16233.

[82] J. Coey, M. Spender and A. Morrish, *Solid State Commun*, 1970, **8**, 1605–1608.

[83] M. R. Spender, J. M. D. Coey and A. H. Morrish, *Can J Phys*, 1972, **50**, 2313 – 2326.

[84] G. W. Watson, E. T. Kelsey, N. H. de Leeuw, D. J. Harris and S. C. Parker, *J Chem Soc Faraday Trans*, 1996, **92**, 433–438.

[85] P. W. Tasker, *Philos Mag A*, 1979, **39**, 119–136.

[86] G. Henkelman and H. Jónsson, *J Chem Phys*, 1999, **111**, 7010–7022.

[87] A. Heyden, A. T. Bell and F. J. Keil, *J Chem Phys*, 2005, **123**, 224101.

[88] N. Hollingsworth, A. Roffey, H.-u. Islam, M. Mercy, A. Roldan, W. Bras, M. Wolthers, C. R. A. Catlow, G. Sankar, G. Hogarth and N. H. de Leeuw, *Chem Mater*, 2014, **26**, 6281–6292.

[89] A. Roldan and N. H. de Leeuw, *Faraday Discuss*, 2017, **197**, 325–336.

[90] B. F. Minaev and H. Ågren, *Collect Czechoslov Chem Commun*, 1995, **60**, 339–371.

[91] A. L. Buchachenko and V. L. Berdinsky, *Russ Chem Rev*, 2004, **73**, 1033–1039.

[92] M. Zhang, R. Yao, H. Jiang, G. Li and Y. Chen, *RSC Adv*, 2017, **7**, 1443–1452.

[93] F. C. Calaza, T.-L. Chen, D. R. Mullins, Y. Xu and S. H. Overbury, *Catal Today*, 2015, **253**, 65–76.